Published in Journal of Marine Systems, 47, issues 1-4, 35-50, 2004
which should be used for any reference to this work

A dynamic model of the Aral Sea water and salt balance

François Benduhn, Philippe Renard*

Centre for Hydrogeology, University of Neuchâtel, 11 Rue Emile Argand, CH-2007 Neuchâtel, Switzerland

Abstract

The Aral Sea is shrinking rapidly since the 1960s mainly because of the diversion of the Amu Darya and Syr Darya rivers for irrigation purposes. Since then, the evaporation became the most important component of the water balance of the Sea and led to a concentration of the remaining salts. In this article, we investigate through a coupled mathematical model of water and salt balance of the Aral Sea, the dynamic evolution of the sea. The water balance considers river inflow, groundwater inflow, atmospheric precipitation and evaporation. The salt balance considers the dominant ions and the chemical precipitation of gypsum, epsomite and mirabilite. The evaporation rates are calculated with a modified Penman equation accounting for the salinity of the lake and using statistical climatic data.

With this model, we obtain an estimate of the evaporation flux (between 1100 and more than 1200 mm/year depending on the salinity) larger than earlier estimates. The estimated groundwater discharge into the sea is also larger than earlier estimates and is highly variable from year to year. The last point is that the model is able to simulate rather well the evolution of the salinity until the 1980s, but it does not reproduce accurately the chemical evolution of the lake during the most recent period and needs further improvements.

Keywords: Dynamic simulation; Water balance; Salt balance; Submarine groundwater discharge; Evaporation; Salt precipitation

1. Introduction

The Aral Sea, formerly the fourth largest lake in the world, is shrinking rapidly since the beginning of the 1960s. Along with the drying out of some 40,000 km^2 of former lake bottom, one observes an important drop down of the groundwater level, as well as salinization of water and soils, endangering every form of human subsistence (Micklin, 1988; Létolle and Mainguet, 1996; Waltham and Sholji, 2001).

* Corresponding author. Tel.: +41-32-718-26-90; fax: +41-32-718-26-03.
E-mail address: philippe.renard@unine.ch (P. Renard).

The Aral Sea results mainly from the discharge of the Amu Darya and the Syr Darya rivers into a large endoreic basin that is enduring an arid or semi-arid climate with high evaporation and low precipitation. Consequently, the Aral Sea is extremely sensitive to the reduction of river inflows that occurred during the last 40 years, mainly because of the intensification of irrigation and cotton cultivation.

During recent geological history, the Aral Sea has known several important periods of rapid shrinking (Boomer et al., 2000). According to these authors, there have been two important regression events during the Holocene (one around 10,000 years BP and another one around 1600 years BP), precisely

Table 1
Mean annual values of the major components of the hydrological budget and morphometric parameters of the Aral Sea (adapted from Bortnik, 1996)

Period	Annual river inflow (km^3)	Annual precipitation (km^3, mm)	Annual evaporation (km^3, mm)	Morphometry at end of period		
				Level (m a.s.l.)	Area (km^2)	Volume (km^3)
1911–1960	56.0	9.1, 138	66.1, 1000	53.4	67,100	1083.0
1961–1970	43.4	8.0, 127	65.4, 1035	51.2	60,200	950.6
1971–1980	16.7	6.3, 110	55.2, 968	45.4	50,800	628.4
1981–1990	4.2	5.5, 143	39.0, 1050	38.6	36,500	328.6

because one of the two tributaries, namely the Amu Darya did not reach the lake any more. During the latter event, the Aral Sea dropped to the same level as in the late 1990s.

To understand the situation and to provide scenarios for mitigation measures, researchers investigated the water and salt balance of the Aral Sea. Many calculations are based on annual water balance. Bortnik (1996) reports that, before 1960, the mean annual components of the balance were approximately 56, 9.1 and 66.1 km^3/year for river inflow, precipitation and evaporation, respectively. The balance was equilibrated; the sea level was oscillating with a mean value of 53.4 m a.s.l. Later, the fluxes dropped rapidly and were around 4.2, 5.5 and 39.0 km^3/year for the river inflow, precipitation and evaporation, respectively, in the 1980s (see Table 1) with a mean level at 38.6 m a.s.l. The groundwater component of the budget is estimated to be between 3 and 5.5 km^3/year depending on the Aral Sea level and the authors (Khodjibaev, 1968; Chernenko, 1987). Glazovsky (1995) considers only the cretaceous and paleogene aquifers and estimates much smaller groundwater fluxes (between 0.07 and 0.27 km^3/year), but he investigates mainly the question of the salt balance. More recently, Small et al. (1999) used a regional climate model coupled with a lake model to estimate the water balance at the lake surface and its influence on local climate. Ferrari et al. (1999) evaluated the effects of artificial and seasonal irrigation as well as of the presence of swamps on the river discharge. Veselov (2002) modelled, in three dimensions, the deep and superficial groundwater flow to the Aral Sea originating from the Tien Shan mountain ranges situated 600 km east of the Aral Sea. His estimate of the groundwater inflow is 0.057 km^3/year for the year 1989. As we see, the question of the amount of groundwater inflow into the Aral Sea is far from solved.

Within this paper, our aim is to provide a tool and new results for the analysis of the groundwater inflow into the Aral Sea. Because we are lacking geological and hydrogeological data, we will adopt an indirect and global approach. We will use a coupled mathematical model of salt and water balance to assess the groundwater discharge from the observed sea level and climatic data. An important effort is devoted to estimating the evaporation rates. The model is inspired from the work of Asmar and Ergenzinger (2002) for the Dead Sea, but is adapted to account, as far as possible, for the specific conditions of the Aral Sea. The main differences between the Dead Sea and the Aral Sea are that the regression is much faster in the case of the Aral, that the salinity of the Aral Sea is much lower than in the Dead Sea and that the chemical composition is different. In the last part of the paper, the model is then used to forecast the possible evolution of the sea according to different scenarios.

2. The mathematical model

The mathematical model consists in two mass balance equations (one for water and one for salts), one evaporation model, one chemical precipitation model and a bathymetric model relating the variations in lake level to lake volume and surface area.

2.1. Water mass balance equation

River discharge, groundwater flow, precipitation, condensation and evaporation are the predominant components of the water balance. The other components, such as storm water inflow or sea spray, are

regarded as negligible. Consequently, the water balance equations are:

$$\frac{dm_w}{dt} = Q_{amu} + Q_{syr} + Q_{gw} + (P + C - E) \times S \quad (1)$$

With m_w representing the total water mass of the Aral Sea, Q_{amu} the mass flux of water from the Amu Darya river, Q_{syr} the corresponding flux from the Syr Darya, Q_{gw} the groundwater flux (including spring discharges), P the precipitation flux per unit area, C the flux of condensation per unit area, E the flux evaporation per unit area and S the surface area of the sea at time t.

In Eq. (1), the precipitation will be considered as essentially a climatic constant determined by statistical analysis of available data. It will allow reducing the importance of punctual data that can be missing for certain years. The net balance of evaporation and condensation (C–E) will be calculated with a modified Penman formula, as it is a function of the salinity of the lake and cannot be kept constant. For the fluvial discharge, we will rely on published annual measurements. For the groundwater flow, either we will fix it to a constant value when we use Eq. (1) to simulate the variation of mass of water in the lake, or we will calculate it by using the measured variation of mass of water within the lake and rewriting Eq. (1) as follows:

$$Q_{gw} = \frac{dm_w}{dt} - Q_{amu} - Q_{syr} + (E - P - C) \times S. \quad (2)$$

2.2. The salt balance equation

The temporal variation of salt mass is the result of salt accumulation from river and groundwater discharge, atmospheric gains minus sea sprays and chemical precipitation processes. The available data concerning the salt mass flux from the Amu Darya and Syr Darya rivers are particularly rough. The salinity of the rivers fluctuates and the chemical composition of the water is intensively affected by irrigation and the use of soil fertilizers, it thus is quite unpredictable. The gains through groundwater and river discharge can be considered together, as both fluxes are likely to be intimately linked. The losses through sea spray and the gains through atmospheric precipitation seem to cancel each other more or less out (Glazovsky, 1995). On the other hand, the amount of certain salt losses increased because of new processes related to the dessication of the lake and responsible for the recent decrease of the total mass of salts in solution. Namely, these processes are: large-scale chemical precipitation through increasing salinity over the entire sea, small-scale precipitation occurring at the boundaries of the lake, salt precipitation in evaporation water pools after their isolation next to the shore. The two latter processes will be called border phenomena. The small-scale precipitation derives from the tendency of shallow water to be more saline due to increased evaporation through a higher water temperature and less intense mixing. A fourth precipitation process concerns calcium carbonate at the river mouths because of water mixing. Assuming that the fluvial salt discharge is of the same order of magnitude as the border phenomena associated with calcium carbonate precipitation, we neglect these fluxes, which would be difficult to estimate. We focus then our analysis on the large-scale precipitation of salts. The subsequent salt mass balance equations is:

$$\frac{dm_{salt}}{dt} = -P_S \quad (3)$$

With m_{salt} the total mass of dissolved salts in the Aral Sea water and P_S the sum of all large-scale chemical precipitation fluxes. Within our assumptions, the total mass of salts can only reduce with time when precipitation occurs due to the concentration of the solution with the reduction of the mass of water.

2.3. Evaluation of the evaporation and condensation

The modified Penman formula used to determine the evaporation and condensation fluxes is (Calder and Neal, 1984):

$$E = \frac{\frac{M_w L_W e_s}{RT_a^2}}{\left(\frac{M_w L_W e_s}{RT_a^2} + \frac{pC_p}{qL_W a}\right)} \frac{H}{L_W} + \frac{pC_p}{qL_W^2} \frac{(e_s - e/a)}{\left(\frac{M_w L_W e_s}{RT_a^2} + \frac{pC_p}{qL_W a}\right)} (0.036 + 0.025u) \quad (4)$$

Where E is the net evaporation flux at the earth's surface per unit surface area, M_W the molecular weight of water, L_W the evaporation enthalpy of water, e_s the partial saturation pressure of water vapour, R the gas constant, T_a the temperature of the air at the earth's surface, p the atmospheric pressure, C_p the specific bulk heat of air at constant pressure, q the molecular weight ratio of water to dry air, a the activity coefficient of water in solution, H the sum of latent and convective heat fluxes at the earth's surface, e the observed partial pressure of water vapour in the atmosphere and u the surface wind velocity.

The constants in the above equation have been used by Asmar and Ergenzinger (1999) for the estimation of evaporation over the Dead Sea. We assume that the aerodynamic conditions of evaporation over the Aral Sea do not differ considerably.

M_W, q, R, L_W and C_p can be taken as constants, e_s is calculated as a function of air temperature, a as a function of the salinity, and T_a, e, u and p are climatic data monthly averaged using meteorological records and supposed to be representative for the Aral Sea.

The formula used to estimate the activity of water is taken from Garrels and Christ (1990):

$$a = 1 - 0.017 \frac{\sum_i (M_s)_i / M_i}{M_w} \tag{5}$$

with M_i the molecular weight of the ion i and M_S the corresponding mass of dissolved ions. Note that this equation is specific to seawater; we did not find a more accurate equation.

H is equal to the part of the net radiation that is returned to the atmosphere, that is the net radiation (R_N) minus the snow and ice melt energy and the net underground exchange energy. Because of a lack of data, we will neglect the difference between R_N and H, and we will estimate R_N through climatic data on the air temperature, the lower and the total cloud cover, and the approximate zenithal angle of the sun as a function of time.

According to Peixoto and Oort (1992), we have at the lake's surface:

$$H \approx R_N \approx \varepsilon L\downarrow + (1 - a_{SW}) S - \varepsilon\sigma T_a^4 \tag{6}$$

With ε=0.95 the emissivity coefficient of water at its surface, $L\downarrow$ the downward longwave radiation, a_{sw} the terrestrial albedo (that is the albedo of water), S the global solar radiation and σ=5.67·10^{-8} W/m^2/K^4, the Boltzmann constant.

For the first and the third term of the previous equation, we have:

$$\varepsilon L\downarrow - \varepsilon\sigma T_a^4 = L\downarrow - (1-\varepsilon) L\downarrow - \varepsilon\sigma T_a^4 = L\downarrow - L\uparrow = \left(\frac{\overline{L\downarrow}}{L\uparrow} - 1\right) L\uparrow$$

Considering that:

$$L\downarrow \approx \frac{\overline{L\downarrow}}{L\uparrow} L\uparrow = 0.8 L\uparrow \tag{8}$$

$$L\uparrow = \varepsilon\sigma T_a^4 + (1-\varepsilon) L\downarrow \tag{9}$$

With $L\uparrow$ the upward longwave radiation flux at the earth's surface.

Combining Eqs. (8) and (9), we can isolate $L\uparrow$ and replace it in Eq. (7). We obtain the following approximation:

$$L\downarrow - L\uparrow = -0.95\sigma T_a^4 \frac{1 - \frac{\overline{L\downarrow}}{L\uparrow}}{1 - (1 - 0.95)\frac{\overline{L\downarrow}}{L\uparrow}} \approx -\left(1 - \frac{\overline{L\downarrow}}{L\uparrow}\right)\sigma T_a^4 = -0.2\sigma T_a^4 \tag{10}$$

Hence, we can express the longwave radiation balance at an aqueous surface as a function of only air surface temperature and the mean ratio of the downward longwave to the shortwave radiation at the earth's surface. Supposing that diffuse light undergoes on average the same alteration through absorption as direct solar radiation, we have the following relationship for the global shortwave radiation:

$$S \approx \cos\varphi \left(q_d^\varphi q_a^\varphi + 0.5\left(1 - q_d^\varphi\right) q_a^\varphi\right) S_0 \tag{11}$$

Where φ is the zenithal angle of the sun, q_a^φ the extinction coefficient through absorption as a function of φ, q_d^φ the extinction coefficient through scattering as a function of φ and S_0 the mean solar constant. The first term of the right hand side of Eq. (11) stands for the direct part of the shortwave radiation at the earth's surface. The second term

represents the diffuse light, assuming that half of the scattered light is directed to the earth's surface, no multiple scattering occurs and the average alteration during the atmospheric transfer is identical to that for direct light, as it is indicated through the unique index φ.

Considering the terrestrial albedo and the effects of clouds, we obtain the following relationship for the global solar radiation absorbed at the earth's surface, that is the second term of Eq. (6):

$$\begin{aligned}(1-a_{SW})S &= 0.5\cos\varphi(1-0.05)q_a^{\varphi}\left(1+q_d^{\varphi}\right)\left[(1-f)\right.\\ &\quad \left.+fq_n^{\varphi}\right]S_0\\ &= 0.475\cos\varphi q_a^{\varphi}\left(1+q_d^{\varphi}\right)\left[(1-f)+fq_n^{\varphi}\right]S_0\end{aligned} \tag{12}$$

With f the fraction of the sky covered by clouds and q_n^{φ} the extinction coefficient of the considered cloud cover.

Albeit the albedo increases significantly for large zenithal angles, we estimated that a large majority of the daily-received shortwave radiation energy corresponds to small zenithal angles. Therefore, the terrestrial albedo will be set to 0.95, which is a typical value for water under these conditions.

The cloud cover is taken into account through the extinction coefficient and the fraction of the sky covered by clouds, that is the probability that direct sunlight has to go through the water droplet layer. Eq. (12) is an example for a unique cloud cover having a typical extinction coefficient. For our model, we shall distinguish between lower and high cover. When the zenithal angle is equal to zero, the extinction coefficients will be put to 0.8 and 0.3, respectively, which are typical values for cirrus clouds. For the same zenithal angle, the extinction coefficient through absorption has been assessed at 0.867, the one through scattering at 0.8372.

The formula used to adapt the extinction coefficients to the actual zenithal angle is given by:

$$q^{\varphi} = \left(q^0\right)^{\frac{x_{\varphi}}{x_0}} \tag{13}$$

Where x_0 is the distance covered by shortwave radiation in the atmosphere at a zenithal angle equal to zero and x_{φ} the same distance at a zenithal angle φ. This latter distance is calculated by a formula.

The only remaining variable to be estimated as a function of local time is the zenithal angle. For this purpose, we have developed an approximate formula that assumes a circular rotational trajectory of the earth:

$$\begin{aligned}\varphi = \arccos\left\{\cos t\cos\lambda\cos\left[\arcsin\left(\sin\beta\sin\left(2\pi\frac{\tau}{P}+\omega\right)\right)\right]\right.\\ \left.-\sin\lambda\sin\beta\sin\left(2\pi\frac{\tau}{P}+\omega\right)\right\}\end{aligned} \tag{14}$$

Where t is the local time, λ the local latitude, β the inclination of the ecliptic, τ the time elapsed since the earth's last crossing of the perihelia, P the terrestrial rotational period and ω the angle given by the spring point and the large axis of the rotational ellipse.

2.4. Salt precipitation

According to Létolle and Mainguet (1996), four salts are likely to precipitate in connection with the present order of magnitude of the salinity and the chemical composition of the Aral Sea: calcium carbonate ($CaCO_3$), gypsum ($CaSO_4{\cdot}2H_2O$), mirabilite ($Na_2SO_4{\cdot}10H_2O$) and epsomite ($MgSO_4{\cdot}7H_2O$).

Precipitation of calcium carbonate occurs essentially next to the Amu Darya and Syr Darya river mouths due to the mixing of the respective river water with sea water. On the other hand, large-scale precipitation of calcium carbonate seems to have a secondary part due to the actual chemical composition of the Aral Sea water (Létolle and Mainguet, 1996). Thus, in accordance with our primary intention to integrate exclusively new large-scale precipitation processes, we decided to neglect carbonate precipitation, which is particularly difficult to estimate due to its close relationship with pH, for which we have no data whatsoever.

Large-scale precipitation of gypsum, as it is documented in the paleolimnology of the lake for the two major two recent shrinking events during the Holocene, constitutes a phenomenon that should have occurred since the 1990s according to the experimental saturation salinity of 30 g/l (Létolle and Mainguet, 1996). We do not dispose of an empirical saturation formula that is specific to the Aral Sea water. We then have recourse to the formula used by Asmar and Ergenzinger (2002) under the Death Sea conditions, which should be more reliable than an analytical formula, which uses activity coefficients.

The solubility of mirabilite is strongly dependent on the temperature of the solution. According to

Létolle and Mainguet (1996), the saturation concentration is 110 g/l (0.34 M) at 10 °C and rises to 930 g/l (2.89 M) at 30 °C. Contrary to mirabilite, for which deposits have been reported in relationship with the 10,000 BP regression event (Létolle and Mainguet, 1996), precipitation of epsomite has not been noticed during studies of the lake's limnology. Hence, precipitation of epsomite seems to occur at higher salinities than for mirabilite.

No empirical formula could be found for the calculation of the saturation concentrations of mirabilite and epsomite. Thus, we use the Davies equation (Butler, 1964):

$$\log_{10}\gamma = -\frac{1.825\cdot 10^6}{(\varepsilon T)^{3/2}}\,|\,(Z+)\cdot(Z-)\,| \times\left(\frac{I^{1/2}}{1+I^{1/2}}-0.2I\right) \tag{15}$$

with γ the activity coefficient of the considered solubility product, ε the dielectric constant, T the temperature of the solution, $Z+$ the ionic charge of the cation, $Z-$ the ionic charge of the anion and I the ionic strength of the solution. The incurred error, when using this estimation approach for the activity coefficient, is inferior to 10% if the solution's total salinity is lower than 0.5 M. For stronger solutions, it might still give an idea of the actual activity coefficient, which is defined by:

$$K_{\mathrm{So}} = [\mathrm{A}]^{v-}[\mathrm{C}]^{v+}\gamma^{[(v+)+(v-)]} \tag{16}$$

Where K_{So} is the solubility constant, [A] the molar saturation concentration of the anion, [C] the corresponding concentration of the cation and $v+/v-$ the respective number of ions per salt molecule.

The estimation principle for quantity of salt precipitated from a saturated solution is given through the example of a salt that is constituted of two ions of equal valence, as it is for epsomite:

$$a = [\mathrm{A}]\cdot[\mathrm{C}]\cdot\gamma^2 \tag{17}$$

$$K_{\mathrm{So}} = [\mathrm{A}]_{\mathrm{e}}\cdot[\mathrm{C}]_{\mathrm{e}}\cdot\gamma_{\mathrm{e}}^2 \tag{18}$$

$$a > K_{\mathrm{So}} \tag{19}$$

$$[\mathrm{A}]-[\mathrm{A}]_{\mathrm{e}} = [\mathrm{C}]-[\mathrm{C}]_{\mathrm{e}} = X \tag{20}$$

With a the observed activity product of the solution and X the precipitated quantity of salt at equilibrium. This latter state is indicated by the index e.

Eq. (17) stands for the measured ion concentrations and the activity coefficient evaluated by the Davies equation. If the solution is saturated, the activity product will be superior to the solubility product (Eq. (18)), as is indicated by Eq. (19).

Combining Eqs. (18) and (20), and assuming that γ is nearly equal to γ_{e}, we obtain for the precipitated quantity of salt:

$$X = 0.5\left\{([\mathrm{A}]+[\mathrm{C}]) - \left(([\mathrm{A}]+[\mathrm{C}])^2 - 4 \times\left([\mathrm{A}][\mathrm{C}]-\frac{K_{\mathrm{So}}}{\gamma^2}\right)\right)^{1/2}\right\}. \tag{21}$$

2.5. Implementation

The salt and water mass balance equations are coded within Matlab. The resulting system of equations is non-linear. A very well-known property of non-linear systems $y=f(x)$ is that the mean of several y values for different x is not the y value corresponding to the mean of x.

$$\bar{y} = \sum_{i=1}^{n} y_i/n = \sum_{i=1}^{n} f(x_i)/n \neq f\left(\sum_{i=1}^{n} x_i/n\right) \tag{22}$$

Consequently, the mean sea level cannot be equal to the level forecasted by using mean climatic and hydrologic forcings. This consideration leads us to use a dynamic model with time steps as small as possible and related to the time scales of the physical phenomena or of the available data. While the time step for the calculation of the evaporation per unit surface is 1 h, it is 5 days for the numerical integration of the mass balance equation.

In addition, when we calculate the groundwater inflows (Eq. (2)), we need to use an iterative method. As a matter of fact, the groundwater inflow influences the surface-related terms of the water balance (Eq. (2)), as it modifies the surface of the lake and its chemical composition, and therefore has an influence on itself. In practice, after 1 year of simulation the calculated level of the

lake is compared to the actual. According to the water balance equations, the difference is attributed to the missing groundwater flow. The simulation is then repeated with the updated groundwater flow until convergence.

As the mass balance equations contain variables of different units, that is mass fluxes (fluvial discharge, groundwater flow), fluxes per unit volume (salt precipitation) and fluxes per unit surface (atmospheric precipitation, evaporation and condensation), we need, in addition, a series of transformation formulas to relate these fluxes with mass variations.

The initial salt and water masses are derived from sea level, salinity per unit volume and some incomplete chemical analyzes of its water. The volume is estimated from the sea level with a polynomial formula based on bathymetric data (more details are given in Section 3.1). Through the volume and the volumetric salinity, we obtain the initial salt mass. The initial water mass is then calculated in two steps. First, we obtain the mass salinity by the iterative solution of the following system of equations:

$$\rho(T, S_{\mathrm{m}}) = A + BS_{\mathrm{m}} + CS_{\mathrm{m}}^{1.5} + DS_{\mathrm{m}}^{2} \tag{23}$$

$$S_{\mathrm{m}} = S_{\mathrm{V}}\rho^{-1} \tag{24}$$

Where ρ is the water density, S_{m} the salinity per unit mass of the solution and S_{V} the salinity per unit volume. A, B, C and D are coefficients depending on the solution temperature given by McCutheon et al. (1993). Finally, the mass of water is related to the volume V of the lake and the mass of salt:

$$m_{\mathrm{w}} = \rho \cdot V - m_S \tag{25}$$

As we obtain S_{m} by dividing the total salt mass by the water mass after every simulation step, the water density can be estimated immediately using Eq. (23) Thanks to the sum of the water and the salt masses and the water density, we can evaluate the lake's volume, and through the bathymetric formulas, we are able to assess the level and the area of the Aral Sea. Hence, we get the freshly assessed surface of the lake that can be integrated in the water balance for the next simulation step.

3. The data

3.1. Bathymetry

The digitized contours of the 1/500,000 bathymetry map of the Institute of Water Problem of USSR (1986) were provided by Montandon (2002). Based on these contours, we interpolated the bathymetry on a grid of an approximate resolution of 400 by 400 m. This digital bathymetry was then integrated in order to obtain the experimental hypsometric curves relating the level of the lake with its volume and surface. In the last step, we used polynomials to represent these curves.

3.2. Aral Sea level

We used mean annual levels published by Chub (2000) for the period of 1960–2001. It is noticeable that the level of the lake shows several characteristic fluctuations, that is a daily periodic fluctuation similar to the sea tides, a chaotic fluctuation due to the atmospheric pressure and wind speed variations, and a seasonal fluctuation reflecting that evaporation is dominant during the summer months while it is dominated by river discharge, precipitation and condensation during wintertime. All these variations complicate the differentiation between mass balance variations and tidal like processes.

3.3. Chemical composition

The largeness of the lake implies that the mixing is insufficient to maintain chemical homogeneity. The disparity between the local meteorological conditions and the mean water residence time is responsible for the chemical composition likely being highly variable and makes the estimation of a mean value necessary. Now, the chemical heterogeneity of the Aral Sea water contrasts with the relative lack of data. Thus, the estimations of the salinity of 1990, for instance, vary from 23.5 to 30 g/l according to Létolle and Mainguet (1996). In practice, we used the two published water compositions in Létolle and Mainguet (1996) for the years 1960 and 1980.

Table 2
Mean meteorological data for certain months illustrating the main tendencies

	January	April	July	October
Mean surface air temperature (°C)	−9.55	7.33	25.45	10.73
Daily temperature variation (°C)	8.70	9.70	11.30	11.45
Partial water vapour pressure (Pa)	291.36	729.60	1760.83	772.50
Total cloud cover fraction (tenths)	0.58	0.47	0.28	0.43
Lower cloud cover fraction (tenths)	0.34	0.18	0.10	0.22
Precipitation (mm)	14.00	12.75	8.00	17.00
Surface wind velocity (m/s)	4.88	5.25	4.75	4.86

3.4. River mouth fluvial discharge

The estimation of the discharge of the Amu Darya and Syr Darya at the respective river mouths is difficult. Indeed, the most proximate respective measurement stations are around 100 km away, and this distance is even lengthening due to the lake's recent regression. The inherent considerable imprecision of any measure of the fluvial discharge adds further to this problem. Consequently, these data, even if they were available, were not directly used in our model. Instead, we used estimates of river discharge at the river mouth from Létolle and Mainguet (1996). For the years 1961–1980, we used 5-year average values; for 1981–1990, we used annual values; and, later on, we used two scenarios (3 and 10 km^3/year).

3.5. Meteorological data

The meteorological data were provided by Montandon (2002). They concern the air temperature, the daily variation of temperature, the steam partial pressure, the total cloud cover fraction, the lower cloud cover fraction, the wind velocity and the precipitation rates. Among the six stations that have been used, four are situated next to the coastline and the two others on

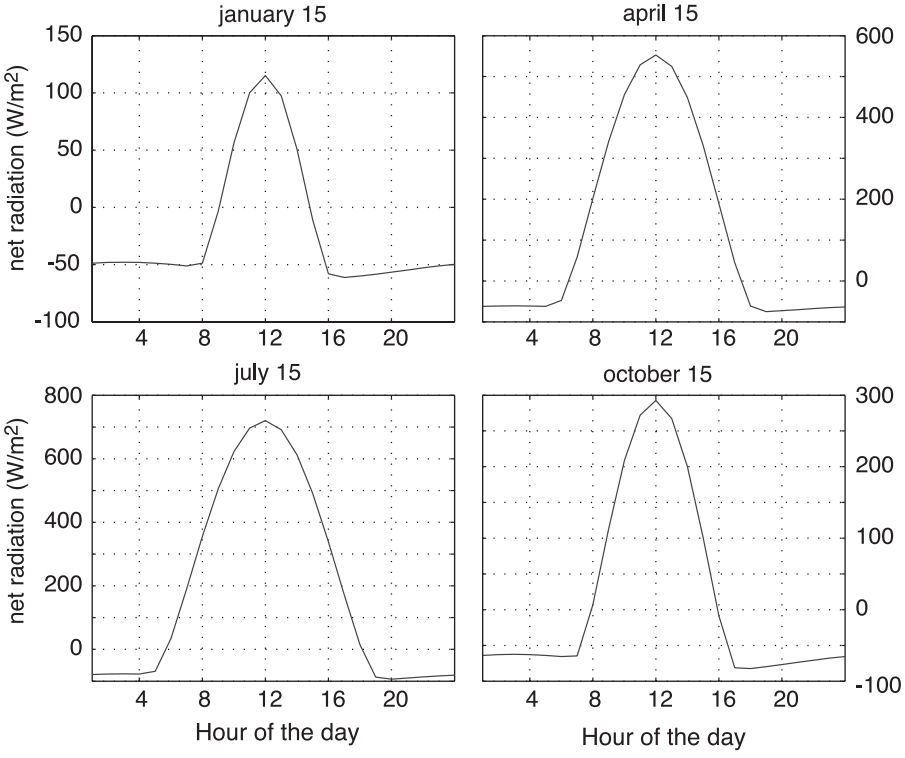

Fig. 1. Example of the calculated hourly net radiation for 4 typical days in winter, spring, summer and fall.

islands. However, due to the lake's regression, the distance between the lake and the stations is increasing and the registered data risks becoming less influenced by the buffering effect of the water mass on local climate. On the other hand, the number of stations is the less sufficient as certain stations do not measure certain values. Consequently, it is impossible to evaluate if the important variability that certain variables show, e.g. the wind velocity and the precipitation, is local, and in that way does not largely concern the average value, or a large-scale phenomenon. When comparing the stations one to another, we were able to notice that, despite the huge standard error, at the 0.95% level some values are not statistically equal. To what extent this disparity was strictly due to microclimatology, which means strictly due to small-scale characteristics could not be determined. Finally, we resolved to estimate climatic values, which are likely to compensate for the restricted number of stations at our disposal as a large temporal interval of data is taken into account, and bear the risk of encountering certain years for which those values are not representative. Table 2 gives the resulting climatic values for some selected months.

4. Results

4.1. Introduction

Four simulations were carried out. The first concerns the 1980s. For this decade, we have initial values for the lake's salinity and chemical composition as well as annual fluvial discharge values at the river mouth. The groundwater water discharge is then calculated iteratively for each of the 10 simulated years. For the second simulation, the mean groundwater discharge of the 1980s is taken as a typical value for the 1960s and 1970s; this allows us to simulate the lake's evolution from 1961 to 1980.

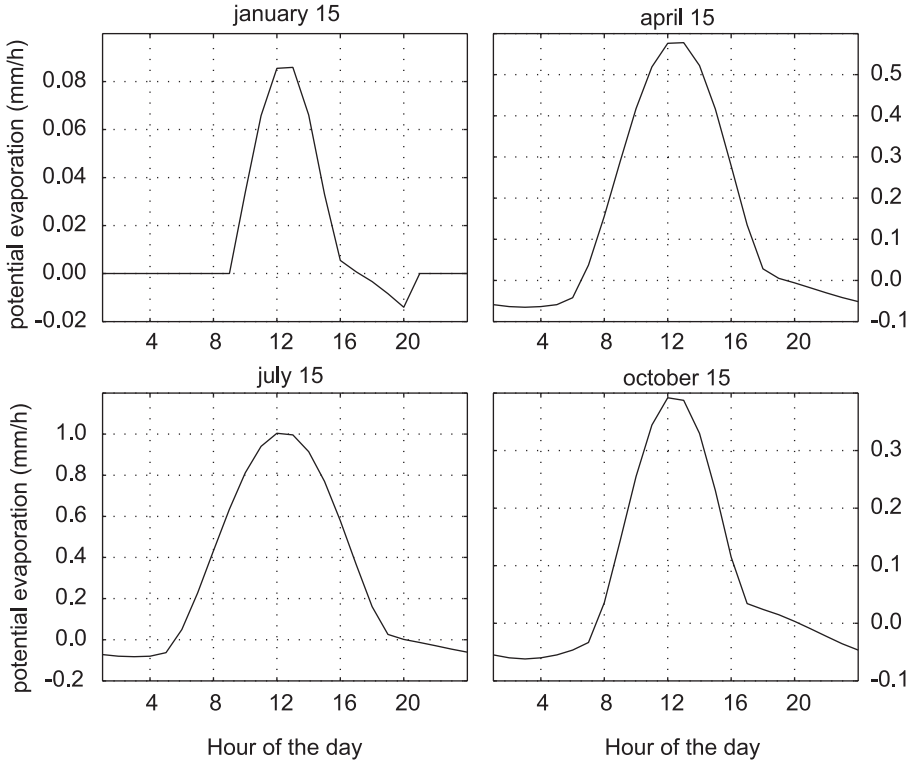

Fig. 2. Example of calculated hourly evaporation for 4 typical days in winter, spring, summer and fall. Note that the negative evaporation corresponds to condensation.

Table 3
Resulting water balance for the 1980s

Year	Level (km)	Area (km^2)°	Volume(km^3)°	Amou-D.	Syr-D.	Evaporation°	Precipitations°	Groundwater	Deficit
1981	0.04518	49,067	590	6.0	1.1	58.3	7.3	15.7	28.2
1982	0.04439	47,669	552	0.0	0.0	56.9	7.1	11.6	38.1
1983	0.04355	46,185	513	0.0	0.0	55.2	6.9	8.9	39.4
1984	0.04275	44,741	476	5.2	0.0	53.4	6.7	5.2	36.3
1985	0.04194	43,274	441	0.0	0.0	51.7	6.5	9.7	35.6
1986	0.04110	41,775	405	0.0	0.0	49.9	6.2	8.0	35.6
1987	0.04029	40,311	372	5.8	0.0	48.2	6.0	3.2	33.1
1988	0.03975	39,311	350	11.8	5.1	46.7	5.8	0.5	23.4
1989	0.03908	38,046	325	0.0	2.9	45.3	5.7	10.9	25.8
1990	0.03824	36,410	293	0.8	1.1	43.6	5.5	5.1	31.1

The fluxes are in km^3/year. The '°' refers to calculations with the model.

The third and fourth simulations are carried out for the period from 1981 to 2020, assuming a fluvial discharge of 3 and 10 km^3/year, respectively. These allowed testing the salt precipitation formulae as well as the model itself, which should converge for both the salt and the water content after a certain time.

4.2. Net radiation and potential evaporation

Figs. 1 and 2 show the calculated daily variations of net radiation and potential evaporation for specific days. The order of magnitude and the variations of the net radiation are plausible. The simulated values are negative during nighttime and positive during daytime. The total annual net radiation is $2.4609 \cdot 10^9$ J, which is similar to the values found in the literature for the lake's latitude. The potential evaporation curves (Fig. 2) follow the net radiation. The annual potential evaporation reaches 1222.8 mm after the subtraction of condensation. According to Létolle and Mainguet (1996), the values estimated so far vary from 950 to 1250 mm/year. Consequently, our simulated value may be in accordance with the actual situation but tends to intensify the arithmetic difference between the observed and the simulated level of the lake. One should note that these results are potential evaporation for fresh water. In the model, the evaporation is recalculated at each time step, since the salinity is evolving.

4.3. Simulation from 1981 to 1990

Table 3 summarizes the annual observed and calculated water balance components. Fig. 3 shows the evolution of the net groundwater discharge as it has been evaluated by iterative calculation according to Eq. (2), in comparison to the fluvial discharge and the losses in the deltas published in Létolle and Mainguet (1996). After three or four iterations, the values converged within 0.01 km^3/year. The groundwater discharge is positive and shows considerable variability, with a minimum value equal to less than 1 km^3 in 1988 and a maximum value of more than 15 km^3 in 1981. The 10-year iterative average value of net groundwater discharge into the Aral Sea is equal to 7.59 km^3/year. For certain years (1982, 1983, 1985 and 1986), the fluvial discharge is equal to zero.

The salinity of the lake in 1981 is responsible for the actual evaporation being reduced to approximately 1176 mm/year. During the 1980s, the effective evap-

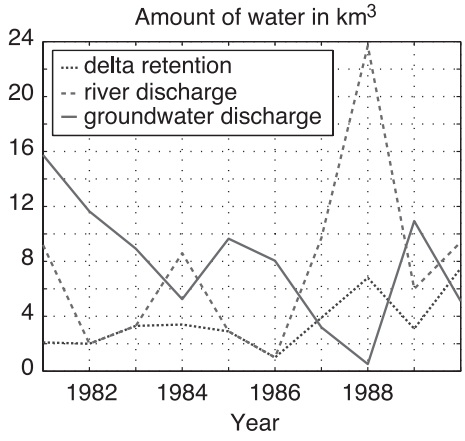

Fig. 3. Estimated annual groundwater discharge into the Aral Sea in comparison to the river discharge at the entry of the deltas and the retention of the deltas.

oration decreases by 6 mm/year, while the simulated salinity increases to 35 g/l. The activity coefficient of water in solution drops from 0.993 to 0.986. Thus, the lake's salinization during the 1980s has hardly affected the actual evaporation, even if the salinity was responsible for a reduction of the effective evaporation by some 50 mm/year when compared to the potential evaporation.

The simulated salinity at the end of the simulation in 1990 is equivalent to 35 g/l. It is significantly higher than the observed one, which is estimated to be from 23.5 to 30 g/l depending on the author (Létolle and Mainguet, 1996). During the period considered, the simulated increase of salinity is exclusively due to the evaporative concentration of the solution, the total amount of salt in solution remains constant. While the observed water mass is more or less equivalent to the simulated one, the higher calculated salinity rules out large-scale precipitation processes and, hence, indicates that the fluvial salt discharge does not compensate the additional losses through boundary phenomena.

4.4. Simulation from 1961 to 1980

Fig. 4 shows the observed evolution of the level of the Aral Sea compared to the simulated level with and without the average groundwater discharge of the 1980s, that is 7.59 km^3/year. The simulated water levels follow rather closely the observations when the groundwater discharge is accounted for, whereas they diverge rapidly when the groundwater flow is neglected. The nearly parallel evolution from 1976 to 1980 seems to indicate that the influence of the variability of the meteorological conditions is low, whereas the disparity during the precedent 15 years is due to the variability of the annual fluvial discharge.

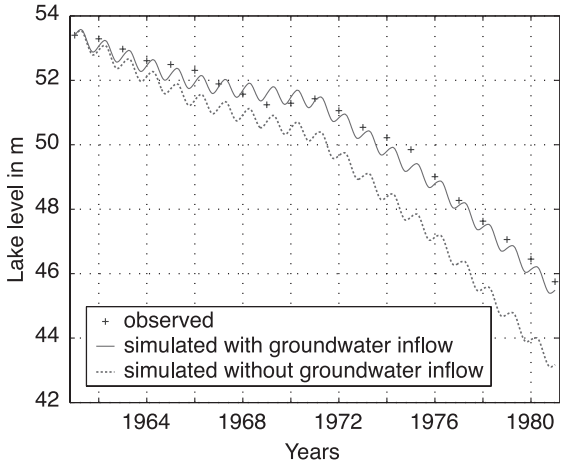

Fig. 4. Simulated evolution of the Aral Sea levels (in meters) in the 1960s and 1970s.

The 1980 simulated salt concentration, which is equal to approximately 17 g/l, is close to the estimated 16.5 g/l according to Létolle and Mainguet (1996). During the simulated time-period, the precipitated salt mass is equal to zero. Consequently, the quantity of salt lost through boundary phenomena seems to be comparable to the losses of the period before 1960; the salt balance remains close to equilibrium.

4.5. Simulation from 1991 to 2020

Fig. 5a shows the evolution of the level of the Aral Sea for a fluvial discharge of 3 and 10 km^3/year from 1991 to 2020, and a groundwater discharge of 7.59 km^3/year. The calculated level is superimposed on the observed level until 2001. The values of fluvial and groundwater discharge are of the same order of magnitude as those of the 1980s. During the 1990s, the observed evolution is similar to the simulated variation of the level of the lake when the fluvial discharge is equal to 10 km^3/year. During the last few years of this decade, however, the actual trend is more pronounced. The Aral Sea seems to be close to its equilibrium state provided that the fluvial regime stays constant, or at least of the same order of magnitude. This equilibrium should be reached by 2020. The corresponding area and volume (Fig. 5b and c) would be within the range of 11,000–17,000 and 70–97 km^3, respectively. The corresponding average residence time is 6–7 years, respectively, while the 1960 original residence time was about 17 years.

The model forecasts an increased influence of the salinity on the evaporation (Fig. 5d). When compared with the 1980s, the evaporation would drop from around 1175 to 1130–1145 mm/year in 2020 depending on the actual average discharge of the rivers. The corresponding activity coefficient of water in solution would be 0.95 and 0.96, respectively.

Fig. 6 illustrates the calculated evolution of the masses of ions in solution provided that fluvial

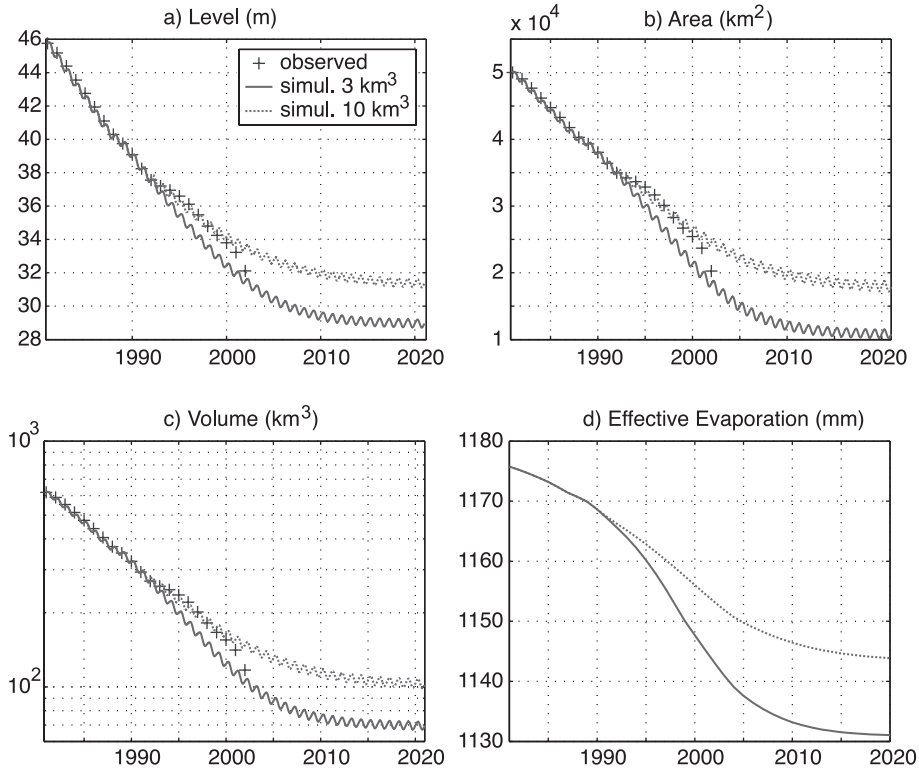

Fig. 5. Simulated evolution of the Aral Sea for a period starting in 1980 and ending in 2021.

discharge is equal to 3 km^3/year following 1991. The calcium mass diminution following summer 1992 testifies to the beginning of simulated gypsum precipitation. The actual precipitation process should have started at an approximate total salinity of 30 g/l at the beginning of the 1990s (see above), whereas the simulated starting salinity is around 40 g/l. Calculated epsomite precipitation occurs for the first time during summer 1999 at a total salinity equal to 70 g/l. Mirabilite precipitation starts during summer 2004 at a salinity equal to 90 g/l. Magnesium and sulfate concentrations are equal to 0.219 and 0.206 M, respectively, at the beginning of the epsomite precipitation. The corresponding sodium and sulfate concentrations for mirabilite are equal to 1.03 and 0.169 M, respectively, and of the same order of magnitude as those predicted above.

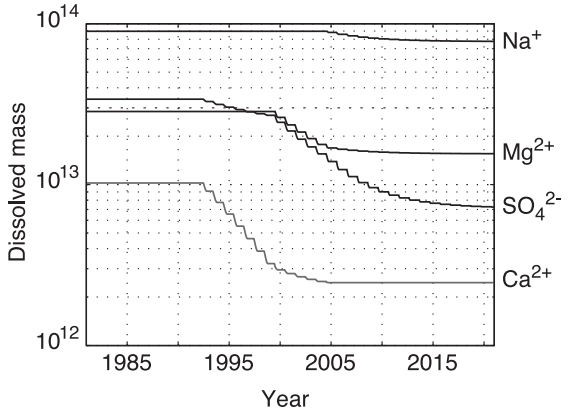

Fig. 6. Simulated evolution of the dissolved masses assuming that the fluvial and groundwater discharge are respectively 3 and 7.59 km^3/year.

5. Discussion

The results presented in the previous section shows that the model reproduces the main trends of lake level and salinity variations. The calculated

evaporation falls within the range of published values, but is in the upper range and larger than the values commonly used in water balance calculations. As a direct consequence, our estimation of the groundwater discharge is also higher and even above the range of published values. However, there are many sources of uncertainty in our model that require discussion.

5.1. Sea separation

During desiccation, the lake tends to separate into pieces. Since the beginning of the 1990s, the Small and the Large Sea are separated and controlled by several episodes of dam construction and breakings. Additional civil engineering work is under planning to separate the western and eastern basins as well as the Adzhibay Gulf (Micklin, 2004). The model does not account for these effects; as a consequence, it assumes implicitly that the river discharges are proportional to the surfaces of the remaining water bodies. This is of course incorrect. Consequently, the model forecasts cannot be accurate, but they still illustrate the possible dynamics of the lake and convergence towards equilibrium.

Because the model does not account for the sea separation and because the Syr Darya has been totally diverted toward the Small Sea, the changes in level predicted with the model are over-estimated for the Large Sea, while they are underestimated for the Small Sea. The predicted salinity is too high for the Small Sea and too low for the Large Sea.

5.2. Evaporation and climate

Evaporation is nowadays the most important water flux. However, it is difficult to determine by direct measurements or calculations. As we will discuss in this section, there are several sources of possible error. The question is whether these errors will lead to an over or underestimation of the evaporation.

The model uses climatic data (data averaged over all the stations and over many years for a given period of the year) and not actual data. This has been done as the hourly and spatial variability over the sea may be important but is thought to be erratic around the mean values. Our opinion is that the climatic data provide a more robust estimation. Assuming the climate is constant, the evaporation rates vary only because of the increased lake salinity.

As the Penman formula is non-linear, we discretized the calculation in hourly intervals. However, the meteorological data are not available at this resolution, except for the temperature. The error resulting from this lack of information is probably moderate as the temperature variation is likely to be dominant and the average wind velocity is essentially a seasonal function. We cannot estimate if this error is positive or negative.

Systematic underestimation of the evaporation may be due to the fact that we do not account for the desiccation of the air masses around the sea due themselves to the desiccation of the sea and climate change. Assuming a homogeneous evaporation rate for the whole surface of the lake, the increased relative influence of the surrounding dry air masses on evaporation is not taken into account. However, when evaluating the typical meteorological data that go into the Penman formula, we already integrated this effect as the majority of the measuring stations that have been retained are situated on the lake's border. As a consequence, we tend to overestimate the evaporation rate from the beginning and, as the lake is shrinking and the relative importance of the borders is increasing, this effect tends to vanish and to be muted into an underestimation.

According to Small et al. (1999), the increase of evaporation through drying of the sea should be negligible when compared to the calculated decrease from the increasing salinity of the lake. These processes account for variations of a few millimeters and several tens of millimeters per year, respectively.

Possible remaining error sources are non-representative mean meteorological data and the modified Penman formula itself, which might be inadequate for the specific aerodynamic conditions over the Aral Sea.

In conclusion, even though many sources of potential error are well identified, it is not possible to define a clear potential systematic error.

5.3. Estimated groundwater discharge and its link to the deltas

The estimated groundwater discharge accuracy suffers from several error sources: estimation of evaporation, measurement of fluvial discharge and

lake level, and use of climatic data to represent the whole lake's surface. Nevertheless, we tried to check (but in any case not to prove) the order of magnitude of the groundwater discharge by analyzing its potential origin.

We consider three possible groundwater origins: (1) the deep groundwater discharge from deep cretaceous aquifers, (2) the dried bottom sediment and (3) the deltaic plains. Both the bottom sediments and the deep groundwater origins can be dismissed through similar arguments. These fluxes are probably quite regular, because they are mainly controlled by deep regional circulation from the Tien Shan recharge area to the Aral depression. These fluxes could increase slightly with the increased hydraulic gradient due to the regular decrease of the lake level during the 1980s, but they should not oscillate over two orders of magnitude as we calculated (Fig. 3).

The groundwater discharge may originate mainly from the deltaic plains. This hypothesis is supported by an apparent negative correlation between fluvial and groundwater discharge (Fig. 3). Yet, the groundwater discharge seems to show a 1–2-year time lag with the fluvial discharge. For example, from 1981 to 1984, there is a continuous decrease of the groundwater flux and then a rise in 1985, just following the rise in 1984 of the fluvial discharge. The amount of water stored in the deltaic aquifers should diminish, as the calculated groundwater discharge is in general greater than the deltas' retention amount estimated previously and published in Létolle and Mainguet (1996). This deltaic aquifer drying process, disrupted temporarily by the 1984 flood, finds support in the dramatic drawdown of the observed groundwater level in the delta regions (Létolle and Mainguet, 1996). However, the orders of magnitude of the calculated flux are rather high and are difficult to understand on the basis of a classical groundwater flux calculation with the Darcy equation for the deltaic plains. A point that merits attention is the fact that precipitations are taken as climatic constants while we know that they can be variable from year to year in arid conditions. The errors due to this assumption are probably not negligible and could explain a part of the variability of the calculated groundwater fluxes. However, with the data available for our study, it was not possible to reduce this potential source of error.

5.4. Salt precipitation

As the simulated precipitation concentration for gypsum is higher by 10 g/l than expected, the solubility formula taken from Asmar and Ergenzinger (2002) seems to be too specific to be applied to the Aral Sea. As the concentrations of sodium and sulfate are of the same order of magnitude as those predicted when precipitation of mirabilite occurs, the Davies equation could be accurate for the estimation of large-scale precipitation processes in the Aral Sea. However, the inverted precipitation order of mirabilite and epsomite seems to reject this hypothesis. In fact, the error encountered with the Davies formula is less than 10% provided that the solutions show a maximum total salinity of 0.5 M, whereas the salinity of the Aral Sea water when precipitation occurs is around 2 M. Consequently, the accuracy of the respective precipitation concentrations must be questioned. Further research and additional data are required to improve our salt precipitation model.

5.5. The water and the salt balance of the Aral Sea

As the salt balance is not simulated accurately as soon as boundary phenomena become dominant, the effect of the salinity on the water balance through evaporation tends to be imprecisely quantified. However, during the 1960s and the 1970s, the boundary phenomena were negligible, large-scale precipitation processes did not yet exist. As a consequence, the salt balance of the lake should still have been in equilibrium, as it was before 1960, and the increase in salinity should exclusively be due to the water losses. In addition, the influence of the salinity on evaporation is relatively low and thus the water balance should be accurately estimated during that period provided that the measured and calculated water fluxes are correct. As we have seen before, the slight difference between the observed and the simulated level of the lake can be attributed to the variability of the river discharge. As the annual evaporation flux is not constant through its dependence on the lake's surface, we encounter another indication that the estimated groundwater discharge values are accurate not only with regard to their variability but also to their order of magnitude. Under the opposite circumstances, the estimated and the observed curves should

diverge as the average groundwater discharge has been determined for the 1980s when the evaporation flux had become less important along with the decreasing surface area. Hence, the average groundwater discharge into the Aral Sea was likely to be fairly constant from 1961 to 1980 and similar to the average value of the 1980s.

The prediction scenarios till 2020 imply under the condition that the fluvial discharge is proportionally partitioned among the remaining water bodies, which the groundwater discharge remains at the same level as in the 1980s. According to our preceding considerations, this is equivalent to an average river discharge of at least 1017 km^3/year, respectively, at the entrance to the deltas as additional losses within these through evaporation have to be expected. As the salinity is likely to be overestimated through the salt balance equation, the evaporation tends to be underestimated, which adds further to the necessary river discharge. Hence, the 3-km^3/year discharge scenario at the river mouths seems to be more realistic when compared to the average values of the 1980s.

6. Conclusion

The mathematical model developed within this paper provides new estimates of the evaporation rates, groundwater discharge and possible evolution of the lake level and salinity.

The estimated evaporation varies between more than 1200 and around 1100 mm/year depending on the salinity of the lake. It is higher than earlier estimations commonly used for Aral Sea water balance calculations. Still, we are confident that the estimated net radiation is correct; however, there are more sources of uncertainty related to the modified Penman equation for the evaporation. A systematic error cannot be excluded.

The estimated groundwater discharge is, as well, higher than previous estimations. It is highly variable in time and correlates with the fluvial discharge at the entry of the deltas. The analysis of these results leads us to conclude that the groundwater component of the Aral Sea is probably dominated by the deltaic aquifer. The deep confined aquifer would play a minor role. The delta aquifers have most probably delayed considerably the shrinking process. Their role in the future evolution of the Aral Sea is still an open question.

The calculated salt budget is satisfying and equilibrated until the 1980s, when boundary phenomena become important. The modeling of the boundary phenomena and the improvement of the salt precipitation model in the main water bodies constitute two possibilities to improve our model in the future.

When we look forward and use our model to forecast the future evolution of the sea, it appears that, if the groundwater and river discharge conditions of the 1980s are maintained, then the Aral Sea should be close to a dynamic equilibrium. Compared to the original state of the lake, the area and the volume of the Aral Sea would be divided by 4 and 10, respectively, while the average water residence time would pass from 17 to 6–7 years approximately. The corresponding salinity should be considerably higher than the corresponding value of Standard Mean Ocean Water.

Acknowledgements

This work was conducted within the SCOPES project no. 7 IP 65663 supported by the Swiss National Science Foundation. The authors gratefully acknowledge L. Montandon and M. Maignan for providing the meteorological and bathymetrical data, as well as R. Létolle and A. Salhokiddinov who provided most of the data that made this research possible.

References

Asmar, B.N., Ergenzinger, P., 1999. Estimation of evaporation from the Dead Sea. Hydrological Processes 13, 2743–2750.

Asmar, B.N., Ergenzinger, P., 2002. Dynamic simulation of the Dead Sea. Advances in Water Resources 25, 263–277.

Boomer, I., Aladin, N., Plotnikov, I., Whatley, R., 2000. The palaeolimnology of the Aral Sea: a review. Quaternary Science Reviews 19, 1259–1278.

Bortnik, V.N., 1996. Changes in water level and hydrological balance of the Aral Sea. In: Micklin, P.P., Williams, W.D. (Eds.), The Aral Sea Basin. NATO ASI Series, Partnership Sub-Series, 2. Environment, vol. 12. Springer-Verlag, Berlin, pp. 25–32.

Butler, J.N., 1964. Ionic equilibrium, a mathematical approach. Addison Wesley, London.

Calder, I.R., Neal, C., 1984. Evaporation from saline lakes: a com-

bination equation approach. Hydrological Sciences-Journal des Sciences Hydrologiques 29, 89–97.

Chernenko, I.M., 1987. More about the Aral Sea problem. Problemy Osvoniâ Pustyn 4, 53–57.

Chub, V.E., 2000. Climate Change and its Impact on the Natural Resources Potential of the Republic of Uzbekistan. SANIGMI, Tashkent. 252 pp. (In Russian).

Ferrari, M.R., Miller, J.R., Russel, G.L., 1999. Modelling the effect of wetlands, flooding and irrigation on river flow: application to the Aral Sea. Water Resources Research 35 (6), 1869–1876.

Garrels, R.M., Christ, C.L., 1990. Solutions, Minerals and Equilibria. Jones and Bartlet, Boston.

Glazovsky, N.F., 1995. The salt balance of the Aral Sea. GeoJournal 35.1, 35–41.

Khodjibaev, N.N., 1968. Ground runoff and the Aral sea problem. Trudy Nauchno-Teknichesgkogo Soveshchaniya po Gidrologi i Inzhnernoi Geologii 1, 53–58.

Létolle, R., Mainguet, M., 1996. Der Aralsee-Eine Ökologische Katastrophe. Springer Verlag, Berlin.

McCutheon, S.C., Matrin, J.L., Barnwell Jr., T.O. 1993. Water quality. In: Maidment, D.R. (Ed.), Handbook of Hydrology. McGraw-Hill, New York, p. 1424.

Micklin, P.P., 1988. Desiccation of the Aral Sea: a water management disaster in the Soviet Union. Science 241, 1170–1176.

Micklin, P.P., 2004. The Aral Sea crisis. In: Nihoul, J., Zavialov, P., Micklin, P.P. (Eds.), NATO Advanced Research Workshop: Dying and Dead Seas, Liège, Belgium, May 8–10, 2003. Kluwer Academic Publishing, Dordrecht.

Montandon, L., 2002. Applications des methods géostatistiques pour l'étude environementale de la region de la mer d'Aral (Asie Centrale). MSc. thesis, University of Lausanne, unpublished.

Peixoto, A.H., Oort, J.P., 1992. Physics of Climate. Springer Verlag, Berlin.

Small, E.E., Sloan, L.C., Hostetler, S., Giorgi, F., 1999. Simulating the water balance of the Aral Sea with a coupled regional climate-lake model. Journal of Geophysical Research 104 (D6), 6583–6602.

Veselov, V., 2002. Simulation of Groundwater Resources of Aral Sea Basin. Institute of Hydrogeology and Hydrophysics of the Ministry of Education and Science, Kazakhstan WWW Page, http://www.aralmodel.unesco.kz.

Waltham, T., Sholji, I., 2001. The demise of the Aral Sea—an environmental disaster. Geology Today 17 (6), 218–224.